Impacts of Pin Fin Shape and Spacing on Heat Transfer and Pressure Losses

Thomas M. Corbett[1]
Department of Mechanical Engineering,
Pennsylvania State University,
State College, PA 16801
e-mail: tmc5980@psu.edu

Karen A. Thole
Department of Mechanical Engineering,
Pennsylvania State University,
State College, PA 16801
e-mail: kthole@psu.edu

Sudhakar Bollapragada
Solar Turbines Incorporated,
San Diego, CA 92101
e-mail: bollapragada_sudhakar@solarturbines.com

Additive manufacturing (AM) provides designers with the freedom to implement many designs that previously would have been costly or difficult to traditionally manufacture. This experimental study leverages this freedom and evaluates several different pin shapes integrated into pin fin arrays of a variety of spacings. Test coupons were manufactured out of Hastelloy-X using direct metal laser sintering and manufacturer-recommended process parameters. After manufacturing, internal surface roughness and as-built accuracy were quantified using Computed Tomography (CT) scans. Results indicated that pin fins were all moderately undersized, and there was significant surface roughness on all interior surfaces. Experimental data indicated that diamond-shaped pins were found to have the highest heat transfer of the tested shapes, but triangle-shaped pins pointed into the flow incurred the smallest pressure drop. Modifications to the streamwise spacing of the pins had little impact on the friction factor, but did increase heat transfer with increasing pin density. Prior Nusselt number correlations found in literature underestimated heat transfer and pressure loss relative to what was measured resulting from the AM roughness. A new correlation was developed accounting for AM roughness on pin fin arrays.
[DOI: 10.1115/1.4056092]

Keyword: heat transfer and film cooling

Introduction

The continued improvement of gas turbine efficiencies is critical with consistent year-to-year growth in commercial air travel expected for the foreseeable future [1] and anticipated increases in demand for electricity generation globally [2]. Developments toward more effective cooling schemes are of particular interest, as they can be integrated into a variety of components to extend the life and reduce the usage of limited cooling air. There have been many technologies that historically been used in turbine cooling, notably ribs, channels, impingement and the focal point of this study, and pin fins [3]. Pin fins for use in turbine cooling, which are well suited for small internal cooling passages, have been studied for decades [4].

Gas turbine components that are exposed to the highest temperatures are typically cast using advanced single-crystal techniques [5–7]. Within these casts, parts are intricate internal cooling features that are often left "as is" without a post-smoothing. The casting can result in increased roughness levels not accounted for in prior studies.

Similar to cast components, additively manufactured (AM) parts also exhibit rough surfaces. AM offers additional advantages, however, being both cheaper and faster than traditional casting when developing one-off parts, as well as providing considerable design freedom. There is interest in how AM roughness impacts on the performance of pin fin arrays as well as how these impacts relate back to the performance expected of cast components. Several prior researchers have explored AM-produced pin fin arrays for gas turbine applications [8,9], though a correlation that can be used to predict the performance of rough-walled arrays has not yet been reported.

This study investigates pin fin arrays featuring a variety of practical streamwise spacings and pin shapes that were produced using AM. After being printed test coupons were evaluated using computed tomography (CT) scans to capture the as-built geometry and roughness and then tested to measure the heat transfer and pressure performance. A new correlation was developed based on the data obtained in this study, as well as from literature, that can be used to predict heat transfer on the basis of pin spacing, Reynolds number, and a new term added to account for roughness in the array.

Literature Review

Early investigations on the performance of pin fin arrays identified the independent impacts that the pins and endwall surfaces had on the total heat transfer. Zukauskas [10] summarized the results from several early pin fin studies that featured long tubes in staggered and in-line formations. Their work identified that the mean heat transfer of such pins could be predicted without considering the endwalls, indicating that the majority of the heat transfer resulted from the pin surfaces. This difference in heat transfer between the pins and endwalls was further explored by Sparrow et al. [11], who found that the heat transfer near the endwalls, was significantly lower than that around the circumference of the pin.

The relative magnitudes of heat transfer from the endwalls and pin surfaces were later found to be a function of the pin height-to-diameter ratio (H/D). A study from VanFossen et al. [12] found that by shrinking the pin H/D to a size relevant to turbine airfoil cooling ($0.5 < H/D < 2$), a greater fraction of the total heat transfer occurred on the endwalls relative to what was seen previously with arrays featuring long pins. They also found that the array-averaged Nusselt number for the low aspect ratio pin fins was smaller than what had previously been reported for longer pins. Brigham and VanFossen [13] continued investigating the effects of the H/D ratio and found that the heat transfer performance of an array is similar when the pin height-to-diameter ratio is between $0.5 < H/D < 2$. Aligning well with these findings, Chyu et al. [14] later determined that the heat transfer coefficient on the endwall surfaces became significantly higher as the pin aspect ratio decreased from $H/D = 4$–2. Later work from Kirsch and

[1]Corresponding author.

Contributed by the International Gas Turbine Institute (IGTI) of ASME for publication in the Journal of Turbomachinery. Manuscript received July 28, 2022; final manuscript received October 18, 2022; published online December 6, 2022. Tech. Editor: David G. Bogard.

Thole [9] investigated additively manufactured low aspect ratio pin fins ($H/D = 1$), featuring rough wetted surfaces. Their work revealed that this roughness increased heat transfer considerably relative to similar geometries with smooth surfaces.

Many studies have focused on investigating the impacts of the spacing of low aspect ratio pin fins in arrays. Multiple studies led by Metzger et al. [15,16] evaluated low aspect ratio pins at several streamwise spacings ($1.5 \le X/D \le 5$). It was found that the heat transfer increased notably with decreases in streamwise spacings within this test range. Both Lawson et al. [17] and Ostanek [18] continued evaluating the changes in performance as a result of pin spacing for low aspect ratio pin fins. Their investigations identified similar patterns of array performance based on their tested streamwise spacing ($1.73 \le X/D \le 3.46$), but additionally found that the spanwise spacing did not have a significant impact on heat transfer within their test range ($2 \le S/D \le 4$) relative to the streamwise spacing. In addition to heat transfer, Lawson et al. and Ostanek captured the array friction factor and found it to be almost entirely a function of spanwise spacing, counter to what was seen for heat transfer. Decreases in spanwise spacing resulted in increases in friction factor within the test range given the greater flow obstruction.

The pin shape also plays a role in heat transfer and pressure loss of the array. Metzger et al. [19] investigated how oblong pins oriented in different directions impacted performance. They found some pin orientations resulted in decreased heat transfer and significant pressure penalties as compared to standard cylindrical pins. Chyu et al. [20] investigated diamond and square-shaped pins finding that both shapes had higher heat transfer than circular pins. The diamond pins were found to incur a higher pressure penalty relative to the square shapes. A later analysis performed by Chyu et al. [21] expanded on these results and found that the diamond and square-shaped pins had similar or lower heat transfer coefficients on the pin as compared to the circular pins. They also found that the two pin shapes induced unique and complex flow fields that improved convective heat transfer on endwalls in the wake region. Note that these studies used smooth surfaces.

Ferster et al. [8] investigated additively manufactured pin fin arrays featuring several different pin shapes at different spacings. They found that certain pin shapes, such as a star and dimpled sphere, imposed a greater pressure penalty than heat transfer benefit as compared to cylindrical pins. Other shapes, however, such as triangle shaped, sustained minimal pressure loss while maintaining heat transfer to that of circular pins.

Several investigators in the past have strived to correlate the heat transfer performance of pin fin arrays using equations of varying complexity. Metzger et al. [16] developed a widely accepted correlation based on the streamwise spacing and pin Reynolds number to determine the array-averaged Nusselt number. This correlation was quickly followed by VanFossen et al. [12], who developed their own correlation using a modified length scale to predict the array average performance. VanFossen's correlation was followed later by groups like Chyu et al. [14], who developed a series of correlations based on the pin aspect ratio. The correlations developed by Chyu et al. were solely a function of the pin Reynolds number and aspect ratio and were therefore independent of the pin spacing. This exclusion was found to result in moderately less accurate prediction of array performance as compared to correlations proposed earlier but did capture the impact of aspect ratio that had not yet been described. Lawson [22] developed a more intricate correlation that used pin spacing as a basis for all equation constants, which was found to improve agreement with experimental data as compared to earlier proposals. Ostanek [18] also developed a correlation that was a function of Reynolds number, streamwise, and spanwise spacings, which showed improved agreement to data collected from several studies.

Previously published papers have identified the impacts of geometric characteristics of pins and spacing of pins with smooth surfaces. In contrast, the study reported in our paper uniquely evaluates the impact of AM roughness by evaluating different pin shapes and spacings. Coupons were characterized to capture true dimensions and surface roughness and then experimentally tested to find the friction factor and heat transfer performance. Using these results, a correlation was developed to predict the performance of several geometries.

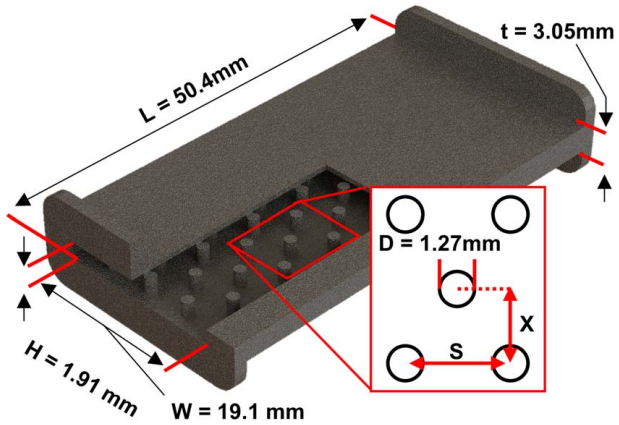

Fig. 1 Test coupon diagram with exposed internal geometry and relevant coupon dimensions

Description of Test Coupons

All pin fin arrays used in this study were packaged into test coupons that were similar in construction to those used in prior studies by one of the coauthors [9,23], as shown in Fig. 1. These test coupons were designed to be 50 mm long, with an internal duct width of 19 mm and a height of 1.9 mm. These duct dimensions resulted in a duct hydraulic diameter (D_h) of 3.46 mm. The thickness of the endwalls was minimized to allow for accurate predictions of heat transfer during experimental testing.

Cylindrical, diamond, and triangle pins were chosen to be investigated for this study. The triangle pins were oriented both with the "point" directed into the flow and in the downstream direction, which are referred to as the point and face orientations, respectively. These shapes were decided based on a previous work by Ferster et al. [8] who analyzed similar pin shapes. The diameter (D) for each of the pin geometries was taken to be the thickness at the point of maximum flow obstruction and was set to be a constant $D = 1.27$ mm across all tested shapes. This definition meant that the pins had a height-to-diameter ratio of $H/D = 1.5$, which is representative of the pin size in engine components. The streamwise spacing of the diamond- and triangle-shaped pins was varied between $2 \le X/D \le 4$, while the spanwise spacing was kept constant at $S/D = 3$. These coupons were intended to be used to explore both the impacts of streamwise spacing and shape. The coupon featuring cylindrical pins was designed to match the spacings from a prior study where $X/D = 2.6$ and $S/D = 4$ [8]. A summary of the pin shape and spacings of the coupons used in this study including roughness is listed in Table 1.

Table 1 Coupon specifications and roughness

Pin shape	X/D	S/D	Endwall R_a/D_h	Pin R_a/D_h
Cylinder	2.6	4	0.0120	0.0100
Triangle point	2	3	0.0119	0.0048
Triangle point	3	3	0.0129	0.0050
Triangle point	4	3	0.0110	0.0028
Triangle face	2	3	0.0119	0.0048
Triangle face	3	3	0.0129	0.0050
Triangle face	4	3	0.0110	0.0028
Diamond	2	3	0.0106	0.0019
Diamond	3	3	0.0133	0.0030
Diamond	4	3	0.0154	0.0018

Coupons were manufactured using an EOS M280 machine out of Hastelloy-X. The coupons were built in the vertical build orientation such that the pins were unsupported inside the ducts. Support structures were used to bind the coupons to the build plate and support the top flanges. The coupons containing triangular pins were constructed such that the point of the triangle pin was pointed downward to allow the pin to be self-supporting. Coupons were manufactured using the process parameters recommended by the manufacturer.

After being printed, coupons were cleared of powder and heat treated to relieve residual stresses from the build. Parts were removed from the build plate, support structures were cut away, and interface surfaces were cut to size using wire electric discharge machining (EDM).

Coupon Characterization

Coupon geometries were characterized using non-destructive CT scans. Scans were completed using a voxel size of 35 μm. Using commercial software, these scans were resolved to one-tenth the voxel size, determining the wall features down to 3.5 μm [24].

Using these scans, the as-built dimensions of the test coupons were captured in a multistep process. The first step was to reconstruct the coupon surfaces from the CT scan using commercial software, followed by exporting these surfaces for analysis using an inhouse code. The inhouse code analyzed the duct diameter by splitting the reconstructed surfaces of the coupon along the flow direction into over 800 slices to determine the perimeter and cross-sectional area for each slice. These measurements were then averaged across all slices to define the measured duct hydraulic diameter. The pin diameters were captured separately by using the scans parsed into over 100 slices along the height of the channel where the perimeter, maximum flow obstruction, and cross-sectional area were captured for each pin in the coupon independently. Once captured, these values were averaged across all pins in a coupon. The pin cross-sectional perimeter and area determined from this analysis were used to calculate the total wetted surface area inside the coupon.

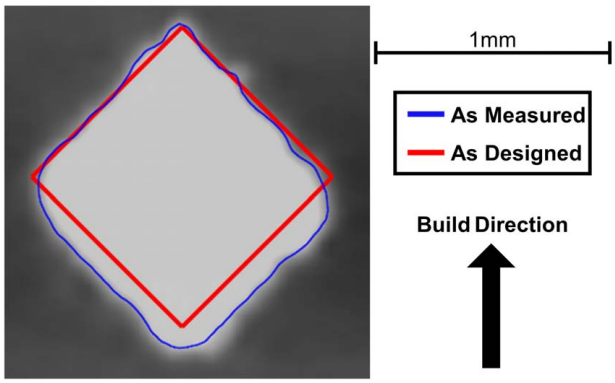

Fig. 2 Accuracy of the as-measured pin to design intent for diamond-shaped pins

Figure 2 showcases the midsection of one of the diamond-shaped pins captured from the CT scans along with the design intent. The unsupported melt pool at the base of the pin permeated lower than intended, thereby lengthening the pin along the build direction. This phenomenon is particularly noticeable at the two spanwise corners, where they become rounded from lack of support functionally reducing the pin's maximum diameter. As a result of this rounding, pin diameters were consistently undersized. The triangle-shaped pins had the most significant deviations while the diamond-shaped pins were printed more accurately.

The interior surfaces of the coupons, as shown in Fig. 3 and indicated in Table 1, were rough for all the geometries built. The endwalls, in particular, had high roughness. The roughness on these surfaces was determined quantitatively using the methods described by Snyder et al. [25]. In short, a plane was fit to the coupon surface, and then, the surface deviation from this plane was measured. These deviations were then averaged to define arithmetic mean roughness (R_a) for a given location. A minimum of four planes were used for each endwall surface in a coupon, with each being approximately one square millimeter in area. The roughness of the pin surfaces and the endwall surfaces were captured independently, and the area-averaged values for both as normalized by the hydraulic diameter are reported in Table 1. Unlike what has been previously reported in literature [9], the area-averaged roughness of these channels was largely the same regardless of pin spacing. This difference is likely a due to the coupon geometry being considerably larger than that which was reported previously, in addition to improved process parameters. It is shown in Table 1 that the pin roughness is between 50% and 90% lower than the roughness on the endwalls. This is likely due to the decreased conduction resistance of the pin surfaces as compared to the thin endwalls which impacted surface morphology during the build.

Experimental Methods

The experimental test facility is similar to that used in previous AM test coupon studies as shown in Fig. 4 [9,26]. During experimental testing, a coupon was installed between two plenums, which conditioned the flow to be uniform as it entered and exhausted from the test coupon. The airflow through the test section was controlled by a mass flow controller located upstream

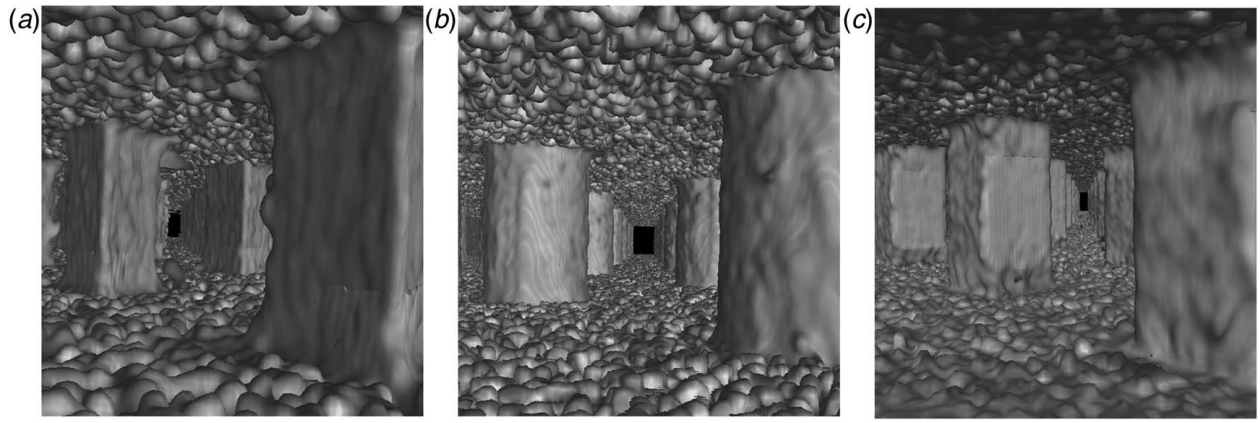

Fig. 3 Internal surfaces of the coupons containing (*a*) triangle pins, (*b*) cylindrical pins, and (c) diamond pins recreated from CT scans

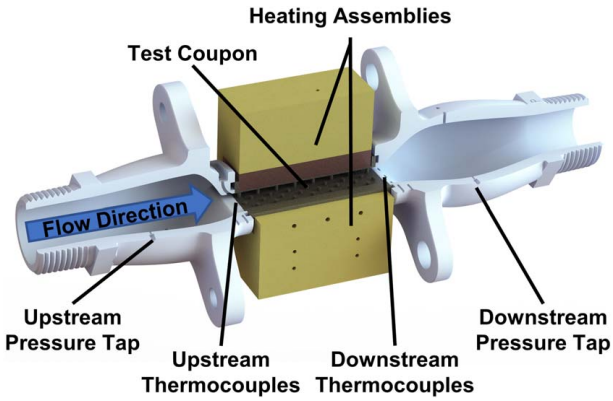

Fig. 4 Diagram of the test section

of the test section. To control the flow pressure in the coupon, a needle valve was used downstream of the test section. Fluid temperatures were captured upstream and downstream of the coupon using several E-type thermocouples. Pressure in the system was captured using an upstream gauge pressure sensor, and pressure drop across the coupon was measured using a differential pressure transducer featuring removable diaphragms to allow for accurate capture of a wide range of pressure drops. Pressure in the test section varied from 15–100 psia depending on the Reynolds number being tested.

For the pin fin studies, the Reynolds number and friction factor were calculated using the minimum flow area through the coupon, which was a function of the spanwise pin spacing, as shown in Eq. (1)

$$U_{\max} = U_{mean}\left(\frac{W}{W - N_{span} \times D}\right) \tag{1}$$

where N_{span} is the number of spanwise pins, W is the channel width, and D is the pin diameter. It should be noted that the Fanning friction factor was used for these studies.

Heat transfer measurements were captured using a constant surface temperature boundary condition with the use of heated copper blocks as shown in Fig. 4. Coupon wall temperatures were constant for a given test and ranged 60–70 °C between tests. Thermal losses were quantified through thermocouples placed throughout the foam blocks and plenums. The heat transfer into the coupon was determined using a one-dimensional conduction analysis based on precisely positioned thermocouples in the copper blocks. This analysis is described in greater detail by Stimpson et al. [26]. The total heat input into the coupon was determined by subtracting the heat that was lost to the surrounding components from the heater power. To ensure that the heat transfer into the system was accurately captured throughout tests, the total heat introduced into the test coupon was compared to the heat calculated using the first law of thermodynamics. This energy balance was found to be within 5% for all tests throughout the range evaluated providing confidence in the measured convective heat transfer.

All sensor data were post-processed using an inhouse code to calculate the temperature, pressure, density, and flow speed at the coupon entrance and exit using one-dimensional (1D) isentropic flow assumptions. The convective coefficient was calculated based on an isothermal wall assumption, which was validated by the high fin efficiency of the array. The convective coefficient is defined in Eq. (2)

$$h = \frac{\sum Q_{in} - \sum Q_{out}}{A_s \Delta T_{lm}} \tag{2}$$

where A_s is the entire wetted surface area of the coupon. The definition of the wetted area is the surface area where the working fluid is touching, and as such, the pin footprint is removed.

To validate the performance of the test rig, it was first benchmarked by collecting data from a smooth traditionally manufactured open channel coupon and comparing the results to known correlations. Friction factor results were validated by comparing them against the laminar flow relation and the Colebrook equation seen as Eq. (3) [27]

$$\frac{1}{\sqrt{f}} = -2\log_{10}\left(\frac{k_s}{3.7D_h} + \frac{2.51}{\mathrm{Re}_{Dh}\sqrt{f}}\right) \tag{3}$$

Because the test coupon was smooth, the Colebrook equation was solved assuming $k_s = 0$ for comparisons against the collected data. It is common practice in pin fin studies to use the Fanning friction factor, which is one-fourth the value for channel flows. As such, all smooth friction factor values determined from the Colebrook equation reported in later sections are divided by four.

Heat transfer measurements were similarly taken using this smooth coupon and were compared against the Gnielinski Correlation as seen in Eq. (4) [28]

$$\mathrm{Nu} = \frac{\frac{f}{8}(\mathrm{Re}_{Dh} - 1000)\mathrm{Pr}}{1 + 12.7\sqrt{\frac{f}{8}}\left(\mathrm{Pr}^{\frac{2}{3}} - 1\right)} \tag{4}$$

The results presented using this correlation were determined using the friction factor for a smooth coupon.

Measurement Uncertainties

Measurement uncertainty was calculated using the method of propagation of error [29]. The largest sources of error in calculating the friction factor were the differential pressure measurements and the measured mass flowrate. The combined uncertainty was approximately 7% for $\mathrm{Re} < 5000$ and 5% or lower for $\mathrm{Re} > 5000$. During testing, several data points were repeated in an overlapping region of pressure diaphragms to ensure measured results were consistent. The repeatability of the friction factor measurements was within 2–4%.

The uncertainty with heat transfer was also quantified with the primary driver being the thermocouples located at the exit of the coupon and the copper blocks, with uncertainties under 7% for the entire test range and results being repeatable within 2%.

Pin Shape Effects

The change in pin geometry had several distinct impacts on the overall performance of the arrays. Figure 5 shows the friction factor as a function of the Reynolds number for coupons of differing pin shapes. Based on the results presented in Fig. 5, it is evident that the flows were fully turbulent throughout the entire test range, as indicated by the friction factor being independent of the Reynolds number. This rapid transition to a turbulent flow is the result of the turbulence induced by the flow interacting with the pins and the rough walls. The triangle pins in the point orientation have the lowest friction factor of the tested shapes, being 36% less than the diamond-shaped pins and 45% less than the triangle pins in the face orientation. This decreased pressure losses for the point orientation are due to two complimentary effects. First, the flow impinging on the pin frontal area is anticipated to play a significant role in the overall pressure losses and this expectation is substantiated by the triangles in the face orientation inducing the highest friction factor. The diamond-shaped pins had the next highest pressure loss, which aligns well with this hypothesis given that the flow through the array had a steeper angle of impact on the diamond pins than on the triangle pins in the point orientation. The second effect is the interactions of the wake regions that occur behind the pins, which has been shown to change depending on pin shape in past literature [21]. While the

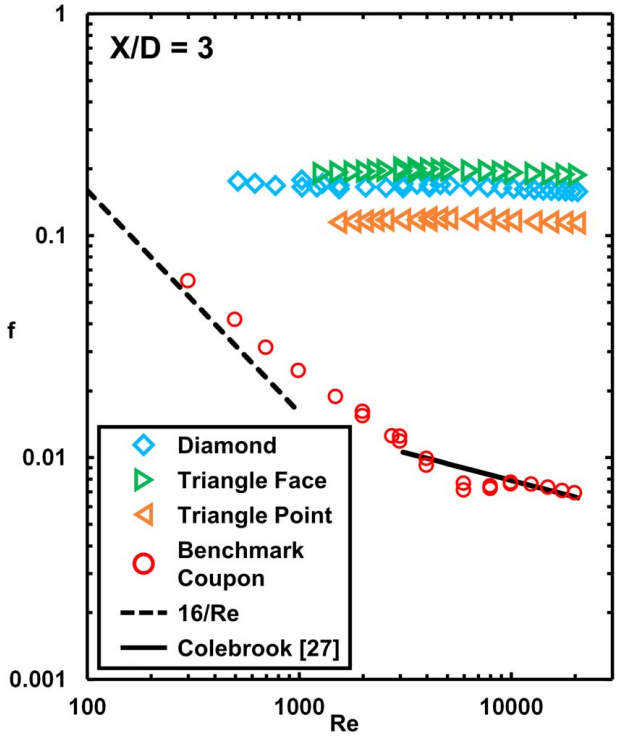

Fig. 5 Friction factor data for coupons of varying pin shape at a streamwise spacing of *X/D* = 3

effects of the wake region have previously been reported to minimally impact friction factor for smooth arrays [17], it is anticipated that the increased endwall roughness for these wake regions is contributing significantly to overall pressure loss.

Figure 6 shows the heat transfer results for the same test coupons that were shown in Fig. 5. As the Reynolds number increases, the difference in performance between the different pin shapes also increases, but the percent difference between the shapes remains largely constant with the diamond-shaped pins performing between 15% and 18% better than the triangles in the point orientation. Aligning with previous research [21], the diamond-shaped pins achieved the highest heat transfer of the tested shapes. This enhancement is augmented further by the increased endwall surface roughness resulting in significantly greater heat transfer than would be expected from smooth pin fin arrays. All pins had similar levels of roughness on the endwall surfaces as shown in Table 1, so the relative differences in heat transfer between these arrays are primarily a function of pin shape.

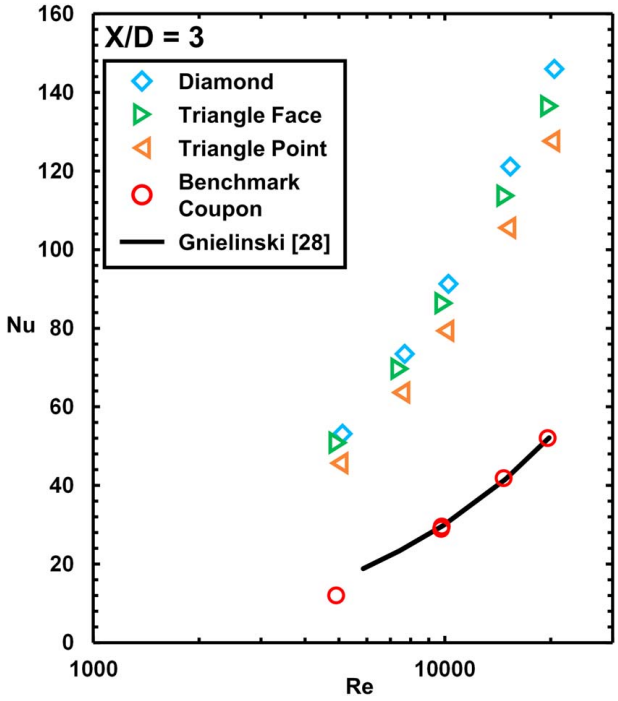

Fig. 6 Nusselt number values for pins of varying shapes at a streamwise spacing of *X/D* = 3

Streamwise Pin Spacing Effects

The friction factors of the coupons at two Reynolds numbers for three different streamwise spacings are shown in Fig. 7, where it can be seen there was minimal variation in friction factor between streamwise spacings. The streamwise spacing effects in this Reynolds regime ($1000 < Re < 20{,}000$) have been shown previously to have little impact on the friction factors for smooth pins as the wake interactions between rows is significantly less influential on pressure drop than the increased flow blockage from decreases in spanwise spacing [17,18]. Conversely, previous AM pin fins have shown that any increase in pin density, either through decreased spanwise or streamwise spacing, resulted in higher friction factors [9]. These heightened friction factors were linked to the increased AM surface roughness, which was also found to increase with tighter spaced arrays. As shown in Table 1, roughness on both the array endwalls and on the pin surfaces was largely the same among the different array geometries. This difference in surface morphology between the current and prior study is likely a function of the increased coupon size, where the current study used a hydraulic duct diameter of 3.5 mm and the prior used test coupons that had a duct diameter of 2.1 mm. Additionally, improvements to the additive process parameters likely played a role in improving these surfaces.

Figure 7 shows that the pin shape and orientation had a much more significant impact on the array performance as compared to streamwise spacing, with the friction factor changing by no more than 6% between spacings for a given Reynolds number and pin shape. In contrast to the friction factors, the array average Nusselt numbers showed more dependence on pin spacing than did the friction factors, as shown in Fig. 8. For example, the tightest spaced diamond pins were able to achieve a 10–15% increase in heat transfer over the

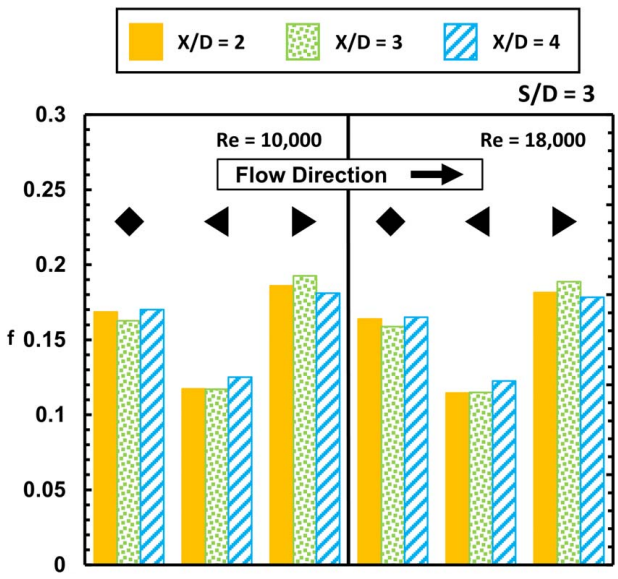

Fig. 7 Friction factor values for pins of varying shape and streamwise spacings at Re = 10,000 and 18,000

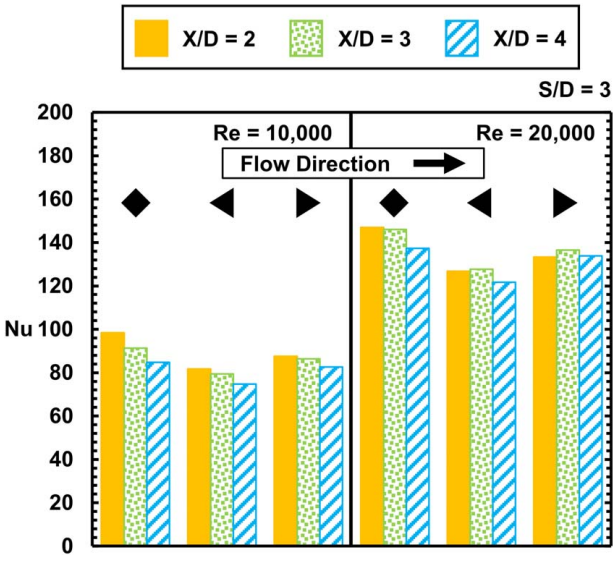

Fig. 8 Nusselt number values for pins of varying shape and streamwise spacings at Re = 10,000 and 20,000

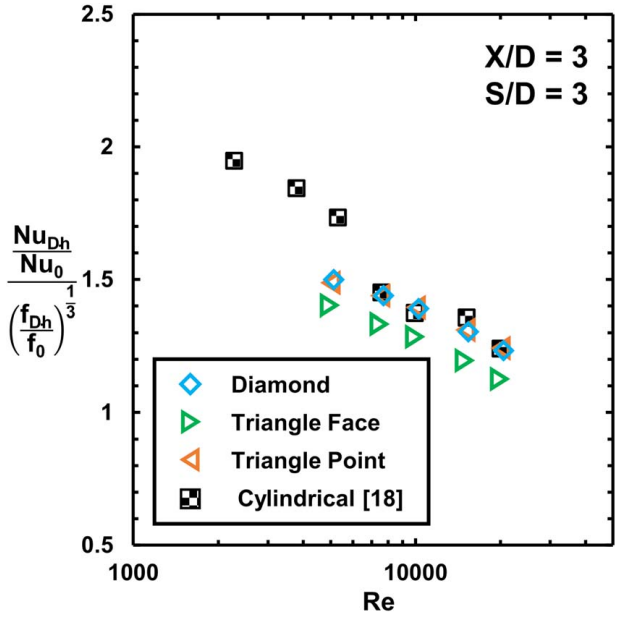

Fig. 9 Efficiency index performance of coupons tested in the current study compared to a traditionally manufactured pin fin array of the same spacing

widest spaced pins at a Re = 10,000. This increase in heat transfer can be attributed to the increased effects of the wake regions behind the pins in the tightest streamwise spacing as compared to the widest as well as the increased surface area. The impact of the increased number of pins becomes less significant as the flow becomes more turbulent, as shown on the right of Fig. 8 at Re = 20,000.

Overall Array Performance

To fully characterize the performance of an internal cooling design, it is important to understand the relative increase in pressure drop compared to the increase in heat transfer. One method of comparison is to determine the efficiency index of the design, which reveals the relative increase in heat transfer performance per increase in required pumping power. The form used in this study was adapted from Gee and Webb [30] and seen as Eq. (5)

$$\eta = \frac{\frac{\mathrm{Nu}_{Dh}}{\mathrm{Nu}_0}}{\left(\frac{f_{Dh}}{f_0}\right)^{\frac{1}{3}}} \tag{5}$$

To appropriately scale the data for this parameter, the Nusselt number was modified to be a function of the duct hydraulic diameter (D_h) rather than pin diameter, and the friction factor for the test coupons was calculated similarly to that of channels, seen as Eqs. (6) and (7)

$$\mathrm{Nu}_{\mathrm{Dh}} = \frac{\mathrm{D_h h}}{\mathrm{k}} \tag{6}$$

$$f_{Dh} = \frac{2\Delta P}{\rho u_{mean}^2}\left(\frac{D_h}{L}\right) \tag{7}$$

This modification to the definitions is required as both the Nusselt number and friction factor are being normalized using the smooth channel correlations shown in Eqs. (3) and (4). Additionally, the values obtained from Eqs. (3) and (4) were calculated using the duct Reynolds number, which uses the duct hydraulic diameter as the length scale. This method for normalizing the Nusselt number and friction factor augmentations is identical to the method used by Ostanek [18].

The efficiency index performance of arrays with diamond- and triangle-shaped pins at a streamwise and spanwise spacing of $X/D = S/D = 3$ is compared to a traditionally manufactured array

Table 2 Geometric characteristics of test coupons

Study	Pin shape	X/D Range	S/D Range	H/D	R_a/D_h
Current study	Varied	2–4	3–4	1.5	0.011–0.015
Kirsch et al. [9]	Cylindrical	1.3–2.6	1.5–4	1	0.039–0.053
Ferster et al. [8]	Varied	1.3–2.6	1.5–4	1	0.040–0.050
Ostanek [18]	Cylindrical	2.16–3.03	2	1	0
Lawson [22]	Cylindrical	1.73–3.46	4	1	0
Metzger et al. [16]	Cylindrical	1–5	2.5	1	0

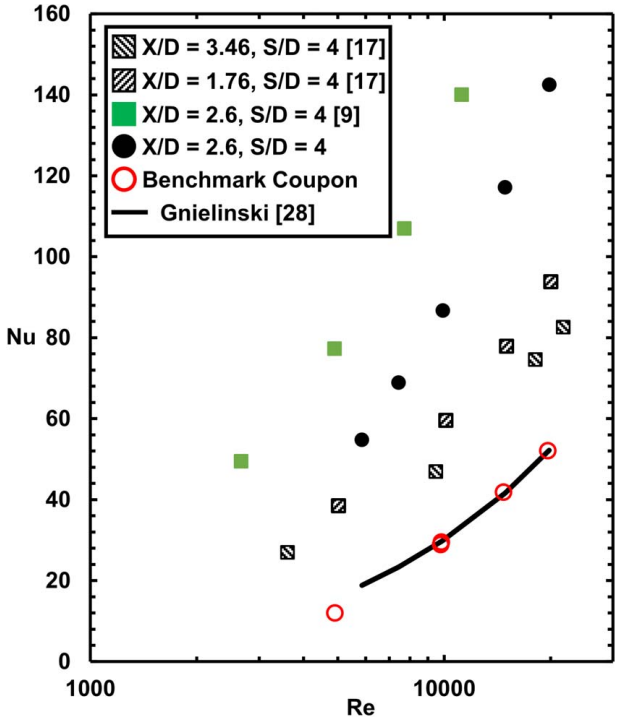

Fig. 10 Nusselt number for various cylindrical pins of similar spacing found in the literature compared to data from the current study

Table 3 Correlation constants

$$\mathrm{Nu} = C_1\left(C_5\left(\frac{R_a}{D_h}\right)^{C_6} + 1\right)\left(\frac{X}{D}\right)^{C_2}\left(\frac{S}{D}\right)^{C_3}\mathrm{Re}^{C_4}$$

C_1	C_2	C_3	C_4	C_5	C_6
0.127	−0.066	0.054	0.657	16.22	0.752

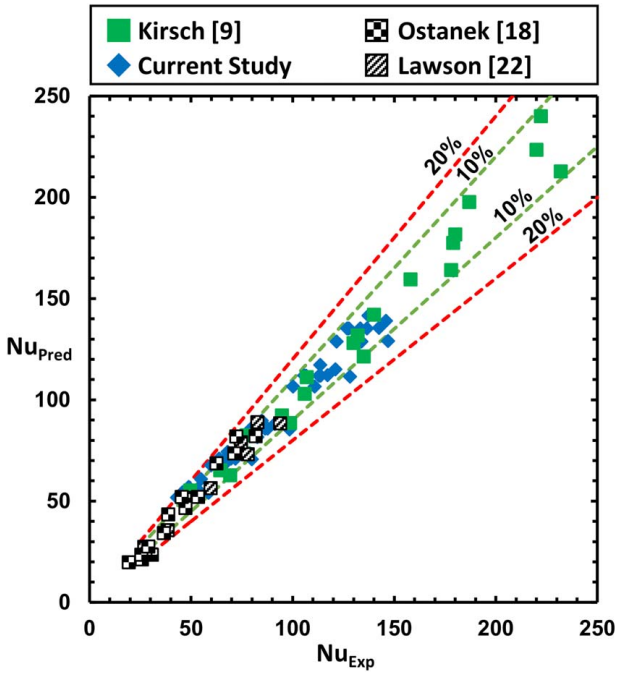

Fig. 11 Prediction accuracy of developed correlation against data in the literature

with cylindrical-shaped pins of the same spacing in Fig. 9. It should be noted that these results are given as a function of the pin Reynolds number, rather than that of the duct Reynolds number. It can be seen in Fig. 9 that the AM coupons perform very similarly to the traditional coupons, despite the AM roughness effects. This indicates that the heat transfer and friction factor are increased proportionally due to the increased surface roughness. However, the triangles pins in the face orientation have a lower efficiency index due to the substantial increase in pressure loss for only moderate increases in heat transfer as the flow impinged on the face of the pin.

Correlating Roughness With Performance

A pin fin array channel containing cylindrical pins was intended to serve as a comparison to prior results from the same laboratory [9,17], but a significant deviation from the prior performance was found. A brief overview of the coupons analyzed in these prior investigations is shown in Table 2, where it should be noted that these studies all used the same definition for Reynolds number, Nusselt number, surface area, and surface roughness. The results indicated measurable differences in Nusselt numbers when comparing the previous coupons with those that were made for this study with both using additive manufacturing. The heat transfer performance for the cylindrical pins is compared to similar array spacings found in literature in Fig. 10. The performance of the coupon developed for this study has significantly lower heat transfer than the previous AM pin fin arrays by Kirsch and Thole [9], but still considerably greater heat transfer from the smooth pin fin arrays (not using AM) by Lawson et al. [17].

The differences in heat transfer shown in Fig. 10 are a result of the significant role the endwall surface roughness has in low aspect ratio pin fin arrays. To compare the roughness effects, the endwall roughness was normalized by the duct hydraulic diameter, D_h, and is reported in Table 2. There was a significant difference in relative roughness between the current and prior AM studies [9,17], with the latter having over twice the relative roughness of the former as shown in Table 2. This increase in heat transfer of small internal passages as a function of relative roughness has been explored previously by Stimpson et al. [31] indicating higher heat transfer with relative roughness. What the results in Fig. 10 also illustrate are the improvements in the additive manufacturing processing parameters with respect to reducing the roughness levels over time by comparing the Kirsch and Thole's [9] study in 2017 to that of the current study in 2021.

In developing a correlation for pin fin arrays with realistic AM roughness levels, prior correlations from the literature were evaluated. Many of the correlations used to predict heat transfer took the form of a common series of multiplied independent variables raised to a constant [14,16,18,22], as seen in Eq. (8)

$$\mathrm{Nu} = C_1\left(\frac{X}{D}\right)^{C_2}\left(\frac{S}{D}\right)^{C_3}\mathrm{Re}^{C_4} \tag{8}$$

where C_1 through C_4 are correlation constants. To account for the relative roughness, an additional term is being proposed by our work to the series, resulting in the modified form seen in Eq. (9)

$$\mathrm{Nu} = C_1\left(C_5\left(\frac{R_a}{D_h}\right)^{C_6} + 1\right)\left(\frac{X}{D}\right)^{C_2}\left(\frac{S}{D}\right)^{C_3}\mathrm{Re}^{C_4} \tag{9}$$

To determine the correlation constants, a non-linear multivariable regression analysis was used on the experimental testing results of the current study including all of the pin fin shapes, as well as all available heat transfer data from the studies by Kirsch et al. [9], Lawson [22], and Ostanek [18]. The objective of the analysis was to minimize the root mean square (RMS) error between the prediction and experimental values. This data set included both additively and traditionally manufactured coupons of a variety of spacings and pin shapes.

Using this method, the constants for the correlation were solved and are shown in Table 3. The predictions using the new correlation are given in Fig. 11. Despite the variations in pin shape, spacing, manufacturing, relative roughness, and size, the correlation can predict heat transfer within 10% for almost all data used to fit the correlation. The correlation is compared against previous work in Table 4, where the valid ranges of geometric characteristics and Reynolds numbers are shown.

To further validate the performance of the correlation, it was used to predict the heat transfer of additional data sets from Ferster et al. [8] and Metzger et al. [16]. The results of this comparison are shown in Fig. 12, where the correlations developed by Chyu et al. [14] and Metzger et al. [16] are also displayed. The previously reported correlations accurately capture the heat transfer of prior smooth coupons for $\mathrm{Re} < 10{,}000$ as shown using various black markers. Likewise, the correlation developed in this study can be seen to predict very similar performance from the smooth pin fins, collapsing almost entirely onto the correlation developed by Chyu et al. [14].

The correlation developed in our study is shown in Fig. 12 to go one step further and predict the heat transfer performance of AM coupons as well indicated with the various colored markers. Notably, the developed correlation shows the ability to accurately predict the performance of various pin shapes despite not including a term to capture this geometric variation. This is due to the relatively small impact that the changes in pin shape had on the heat transfer performance as compared to the large changes that were the result of the increased endwall roughness.

While not reported in this particular study due to the unavailability of published data, it is expected that this correlation could be used to predict the heat transfer of traditionally rough-cast components as well. Given the sensitivity of heat transfer to relative

Table 4 Correlations for pin fin array heat transfer

Study	Pin shape	*X/D*	*S/D*	*H/D*	Reynolds	Correlation
Metzger et al. [16]	Cylindrical	1.5–5.0	2.5	0.5–3	2,000–100,000	$\mathrm{Nu}_D = 0.135\left(\frac{X}{D}\right)^{-0.34}\mathrm{Re}_D^{0.69}$
Chyu et al. [14]	Cylindrical	2.5	2.5	1	10,000–30,000	$\mathrm{Nu}_D = 0.14\mathrm{Re}_D^{0.65}$
Ostanek [18]	Cylindrical	2.16–3.03	2–3	1	1,000–100,000	$\mathrm{Nu}_D = 0.41\left(\frac{X}{D}\right)^{-0.2}\left(\frac{S}{D}\right)^{-0.26}\mathrm{Re}_D^{0.57}$
Lawson [22]	Cylindrical	1.73–3.46	2–4	1	5,000–25,000	$\mathrm{Nu}_D = \left[0.128\left(\frac{S}{D}\right)^{0.165}\left(\frac{X}{D}\right)^{-0.310\left(\frac{S}{D}\right)+1.182}\right]\hat{\mathrm{Re}}_D\left[0.680\left(\frac{S}{D}\right)^{-0.023}\left(\frac{X}{D}\right)^{0.048\left(\frac{S}{D}\right)-0.224}\right]$
Current Study	Varied	2–4	2–4	1–2	2,000–50,000	$\mathrm{Nu}_D = 0.127\left(16.22\left(\frac{R_a}{D_h}\right)^{0.752}+1\right)\left(\frac{X}{D}\right)^{-0.066}\left(\frac{S}{D}\right)^{0.054}\mathrm{Re}_D^{0.657}$

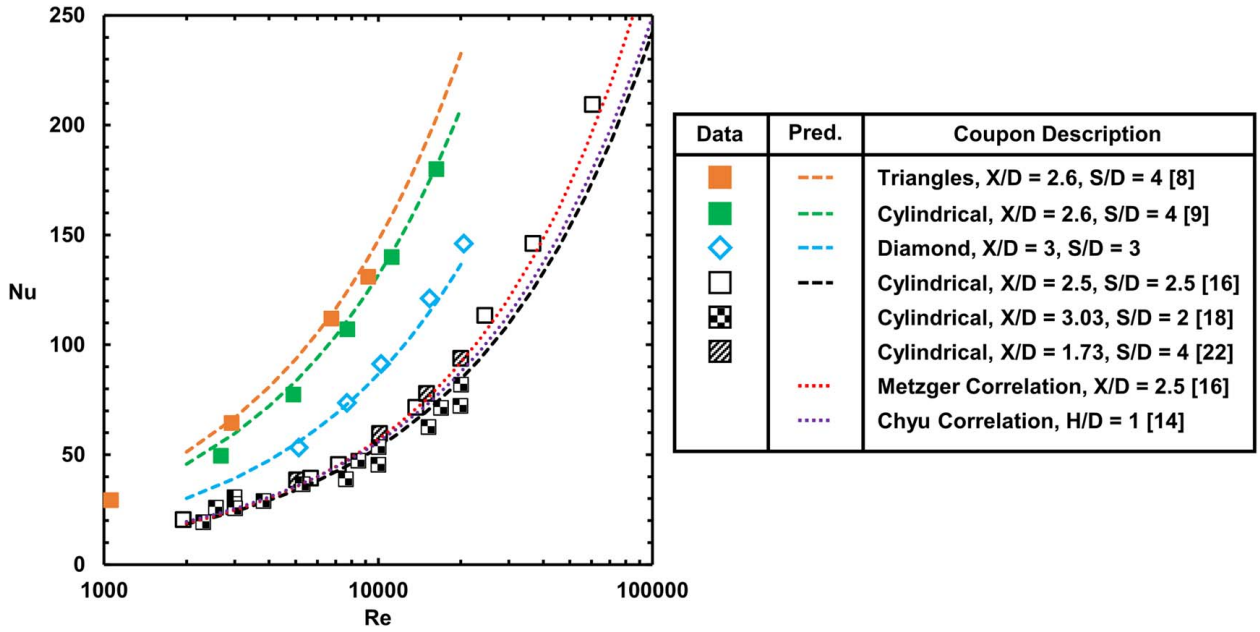

Fig. 12 Developed Nusselt number correlation compared to data and correlations found in the literature

roughness, having a correlation that includes one such term can be highly useful for engineers designing components exposed to high thermal loads. This correlation can be employed as a way of scaling the performance of prototypes made through additive manufacturing to final cast components.

Conclusions

The current study investigated the impacts of three elements of pin fin array design: pin geometry, spacing, and surface roughness. Several pin fin array designs were packaged into additively manufactured test coupons with these parameters varied and experimentally tested. Geometric characterization showed that pins were able to be largely accurately reproduced, though pins were all slightly undersized. The characterization of the coupons also revealed higher surface roughness on array endwalls relative to the roughness on the pins.

Experimental results indicated that the triangle-shaped pins with their point directed into the flow resulted in the lowest overall friction factor, whereas reversing the triangle orientation resulted in the highest friction factor. The highest heat transfer was achieved by the diamond-shaped pins, likely as a result of the increased levels of turbulence in the wake region, which were further enhanced by the rough endwalls. It was shown that pin streamwise spacing had a little overall impact on the friction factor in the ranges tested, which is a result of the relative roughness dominating spacing effects as contributors to the friction factor. The heat transfer was found to slightly increase with tighter spaced coupons at low Reynolds numbers. The efficiency index for the additively manufactured pin fin arrays was shown to be the same as traditionally manufactured arrays for a range of Reynolds numbers, indicating that the ratio of heat transfer benefit to pressure loss is similar for both AM and traditional arrays.

Correlations in literature for heat transfer were found to significantly underpredict the heat transfer performance of the additively manufactured pin fin arrays because of the roughness. Comparisons of the data in the literature showed a significant relationship between Nusselt number and relative roughness. To account for the roughness, a new correlation was developed with an additional term to capture the impact of the relative roughness of the array. This correlation was developed such that it can be used to predict the heat transfer of both highly rough and smooth pin fin arrays of a variety of spacings and shapes.

As additive manufacturing continues to prove to be a valuable asset in prototyping and cooling design development, it is critical to understand how the as-built geometry impacts pin fin array performance. Furthermore, it is essential that designers have the required tools to predict the performance of these arrays, so that comparisons between manufacturing methods can be made before going through the manufacturing process. The results presented in this study bridge this gap so that designers can more effectively use AM in gas turbine cooling design.

Acknowledgment

The authors of this study would like to thank Solar Turbines Incorporated whose support made this work possible. Their insight into the project gave valuable commercial perspective. Additional thanks to Corey Dickman and CIMP-3D for their assistance in developing and printing AM coupons, as well as Whitney Yetter and Penn State's CQI for conducting all CT scans used to analyze test coupons.

Conflict of Interest

There are no conflicts of interest.

Data Availability Statement

The data sets generated and supporting the findings of this article are obtainable from the corresponding author upon reasonable request.

Nomenclature

f = Fanning friction factor, $f = \frac{\Delta P}{2\,\rho u_{max}^2}\frac{1}{N_{row}}$

h = convective heat transfer coefficient, $h = \frac{Q_{in} - \sum Q_{loss}}{A_s \cdot \Delta T_{lm}}$

k = thermal conductivity

p = perimeter

D = pin diameter

H = coupon duct height

L = duct length

P = static pressure

Q = heat transfer rate

S = spanwise distance

T = temperature

W = coupon duct width

X = streamwise distance

A_c = cross-sectional flow area

A_s = surface area

D_h = hydraulic diameter, $D_h = 4\frac{A_c}{p}$

N_{row} = number of streamwise rows of pins

N_{span} = number of pins in the spanwise direction

R_a = arithmetic mean surface roughness, $R_a = \frac{1}{n}\sum_{i=1}^{n}|z_{surf} - z_{ref}|$

T_{LM} = log-mean temperature, $\Delta T_{LM} = \frac{T_{in} - T_{out}}{\ln\left(\frac{T_s - T_{in}}{T_s - T_{out}}\right)}$

U_{mean} = mass average velocity at coupon inlet

Nu = Nusselt number, $Nu = h\frac{D}{k_{air}}$

Pr = Prandtl number

Re = Reynolds number, $Re = \frac{u_{max}D}{\nu}$

Greek Symbols

ρ = fluid density

ν = kinematic viscosity

Subscripts

in = inlet condition

max = maximum condition

out = outlet condition

References

[1] IATA, 2021, Industry Statistics Fact Sheet 2021, Montreal, Canada.
[2] International Energy Agency, 2021, Global Energy Review 2021, International Energy Agency, Paris, France.
[3] Ligrani, P., 2013, "Heat Transfer Augmentation Technologies for Internal Cooling of Turbine Components of Gas Turbine Engines," Int. J. Rotating Mach., **2013**, pp. 1–32.
[4] Armstrong, J., and Winstanley, D., 1988, "A Review of Staggered Array Pin Fin Heat Transfer for Turbine Cooling Applications," ASME J. Turbomach., **110**(1), pp. 94–103.
[5] Gülen, S. C., 2019, *Gas Turbines for Electric Power Generation*, Cambridge University Press, New York.
[6] Schilke, P. W., 2004, *Advanced Gas Turbine Materials and Coatings.*, General Electric Company, Schenectady, NY.
[7] Konter, M., and Thumann, M., 2001, "Materials and Manufacturing of Advanced Industrial Gas Turbine Components," J. Mater. Process. Technol., **117**(3), pp. 386–390.
[8] Ferster, K. K., Kirsch, K. L., and Thole, K. A., 2018, "Effects of Geometry, Spacing, and Number of Pin Fins in Additively Manufactured Microchannel Pin Fin Arrays," ASME J. Turbomach., **140**(1), p. 011007.
[9] Kirsch, K. L., and Thole, K. A., 2017, "Pressure Loss and Heat Transfer Performance for Additively and Conventionally Manufactured Pin Fin Arrays," Int. J. Heat Mass Transfer, **108**, pp. 2502–2513.
[10] Zukauskas, A., 1972, "Heat Transfer From Tubes in Cross Flow," Adv. Heat Transfer, **8**, pp. 93–160.
[11] Sparrow, E. M., Stahl, T. J., and Traub, P., 1984, "Heat Transfer Adjacent to the Attached End of a Cylinder in Crossflow," Int. J. Heat Mass Transfer, **27**(2), pp. 233–242.
[12] VanFossen, G. J., 1981, "Heat Transfer Coefficients for Staggered Arrays of Short Pin Fins," ASME. J. Eng. Power, **104**(2), pp. 269–274.
[13] Brigham, B. A., and VanFossen, G. J., 1984, "Length to Diameter Ratio and Row Number Effects in Short Pin Fin Heat Transfer," ASME J. Eng. Gas Turbines Power, **106**(1), pp. 241–244.
[14] Chyu, M. K., Siw, S. C., and Moon, H. K., 2009, "Effects of Height-to-Diameter Ratio of Pin Element on Heat Transfer From Staggered Pin-Fin Arrays," Paper No. GT2009-59814.
[15] Metzger, D. E., Berry, R. A., and Bronson, J. P., 1982, "Developing Heat Transfer in Rectangular Ducts With Arrays of Short Pin Fins," ASME J. Heat Transfer-Trans. ASME, **104**(4), pp. 700–706.
[16] Metzger, D. E., Shepard, W. B., and Haley, S. W., 1986, "Row Resolved Heat Transfer Variations in Pin-Fin Arrays Including Effects of Non-Uniform Arrays and Flow Convergence," Paper No. 86-GT-132, American Society of Mechanical Engineers, pp. 1–7.
[17] Lawson, S. A., Thrift, A. A., Thole, K. A., and Kohli, A., 2011, "Heat Transfer From Multiple Row Arrays of Low Aspect Ratio Pin Fins," Int. J. Heat Mass Transfer, **54**(17–18), pp. 4099–4109.
[18] Ostanek, J. K., 2012, "Flowfield Interactions in Low Aspect Ratio Pin-Fin Arrays," PhD diss., The Pennslyvania State University, State College, PA.
[19] Metzger, D. E., Fan, C. S., and Haley, S. W., 1984, "Effects of Pin Shape and Array Orientation on Heat Transfer and Pressure Loss in Pin Fin Arrays," ASME J. Eng. Gas Turbines Power, **106**(1), pp. 252–257.
[20] Chyu, M. K., Hsing, Y. C., and Natarajan, V., 1998, "Convective Heat Transfer of Cubic Fin Arrays in a Narrow Channel," ASME J. Turbomach., **120**(2), pp. 362–367.
[21] Chyu, M. K., Yen, C. H., and Siw, S., 2007, "Comparison of Heat Transfer From Staggered Pin Fin Arrays with Circular, Cubic and Diamond-Shaped Elements, Paper No. GT2007-28306, pp. 1–9.
[22] Lawson, S. A., 2007, "Heat Transfer From Multiple Row Arrays of Low Aspect Ratio Pin Fins," Virginia Polytechnic Institute and State University, Blacksburg, VA.
[23] Wildgoose, A. J., Thole, K. A., Sanders, P., and Wang, L., 2021, "Impact of Additive Manufacturing on Internal Cooling Channels With Varying Diameters and Build Directions," ASME J. Turbomach., **143**(7), p. 071003.
[24] Reinhart, C., 2011, *Industrial CT & Precision*, Heidelberg, Germany.
[25] Snyder, J. C., Stimpson, C. K., Thole, K. A., and Mongillo, D. J., 2015, "Build Direction Effects on Microchannel Tolerance and Surface Roughness," ASME J. Mech. Des., **137**(11), p. 111411.
[26] Stimpson, C. K., Snyder, J. C., Thole, K. A., and Mongillo, D., 2016, "Roughness Effects on Flow and Heat Transfer for Additively Manufactured Channels," ASME J. Turbomach., **138**(5), p. 051008.
[27] Colebrook, C. F., 1939, "Turbulent Flow in Pipes, With Particular Reference To the Transition Region Between the Smooth and Rough Pipe Laws," J. Inst. Civ. Eng., **12**(8), pp. 393–422.
[28] Gnielinski, V., 1975, "New Equations for Heat and Mass Transfer in the Turbulent Flow in Pipes and Channels," NASA STI/Recon Tech. Rep. A, **41**(1), pp. 8–16.
[29] Dunn, P. F., 2014, *Measurement and Data Analysis for Engineering and Science*, CRC Press, Boca Raton, FL.
[30] Gee, D. L., and Webb, R. L., 1980, "Forced Convection Heat Transfer in Helically Rib-Roughened Tubes," Int. J. Heat Mass Transfer, **23**(8), pp. 1127–1136.
[31] Stimpson, C. K., Snyder, J. C., Thole, K. A., and Mongillo, D., 2017, "Scaling Roughness Effects on Pressure Loss and Heat Transfer of Additively Manufactured Channels," ASME J. Turbomach., **139**(2), p. 021003.